STARVATION KINETICS OF OSCILLATING MICROBIAL POPULATIONS

A.C. Fowler
MACSI, University of Limerick, Limerick
and
OCIAM, University of Oxford

[Accepted 24 February 2014. Published 25 July 2014.]

Abstract

We study the dynamics of a model which is perhaps the simplest one which describes the competition between different classes of bacteria competing for the same resource. The competition is not entirely antagonistic but is partly syntrophic, resulting in a model which has aspects of activator–inhibitor kinetics, and which exhibits oscillations. In conditions of starvation, these oscillations are extreme, resulting in boom-and-bust dynamics in which there are concentrated population spikes interspersed by extremely low population levels. In practice, continuous models become inappropriate at such low levels, and a stochastic generalisation allows the possibility of extinction. We explain why these results occur, and we give an asymptotic and numerical description of the resulting dynamics of the solutions. This description is likely to be generally applicable to systems exhibiting autocatalytic oscillation, and we suggest that for a larger number of such interacting populations, the solutions may exhibit multiple spiking events.

1. Introduction

Oscillations which occur in the form of periodic spikes or pulses occur in a number of different fields of application, many of them associated with the explosive growth and decline of populations. Examples include epidemic outbreaks (Kermack and McKendrick ([11])), plankton blooms (Mahadevan *et al.* ([15])), glycolytic oscillations ([8]), and paleoclimatic calcification spikes ([21]). Similar low minima spiking oscillations occur in the Lorenz equations at high σ ([6]) and the delayed logistic equation ([3]), and the extremely low minima which can be obtained in these models, even when the causative small parameter is not actually that small, may for example explain the efficiency of the immune system in annihilating infections ([2]).

It is therefore of interest to understand the cause and nature of such oscillations, and in particular the analytic reasons which cause the asymptotically low minima which occur. One particular class of processes which can lead to spiking oscillations is a class of autocatalytic models identified by Omta *et al.* ([21]), which in its

*E-mail: andrew.fowler@ul.ie

doi:10.3318/PRIA.2014.114.09

Cite as follows: A.C. Fowler, Starvation kinetics of oscillating microbial populations, *Mathematical Proceedings of the Royal Irish Academy* **114A** (2014), 173–189; doi:10.3318/PRIA.2014.114.09

simplest form is represented by the reaction

$$\overset{S}{\rightarrow} C + H \overset{k}{\rightarrow} (1+Y)H \overset{d}{\rightarrow} . \tag{1.1}$$

Similar kinds of system have been studied by Gray and Scott ([9, p. 221]) and particularly Goldbeter ([8, p. 43])(see also Keyner and Sneyd [10, p. 23]). The same process has been described by Sanchez-Vila *et al.* ([24]), with application to microbial populations. This reaction describes a population H which grows by feeding on a nutrient C which is supplied at a rate S; the population dies at a rate d. Mass action kinetics applied to this scheme yields the pair of equations

$$\begin{aligned} \dot{H} &= kYHC - dH, \\ \dot{C} &= S - kHC. \end{aligned} \tag{1.2}$$

It is more common to use Monod kinetics for the rates, as was done by Fowler *et al.* ([7]), where the coefficient k in (1.2) would be replaced by $kC_0/(C_0 + C)$, but the difference is entirely one of algebraic detail in (1.5) below and its analysis ([4]), as is easily shown.

It would be of interest to be able to realise this system experimentally. Essentially what is needed is a continuous stirred tank reactor with input of C and removal of H but not C. The simplest way to do this, at least for a microbe/nutrient system, is by having a semi-permeable membrane at the exit pipe, which allows the removal of planktonic bacteria but not the nutrient. This requires the nutrient particles to be large (possibly by using nutrient-coated inert particles), and there is then a difficulty of clogging of the outlet, though this may be resolved by using light particles and vigorous stirring (which is in any case necessary to prevent biofilm formation).

The nature of the solutions of (1.2) is easily understood by defining

$$H = \frac{YS}{d} e^{\theta}, \tag{1.3}$$

and scaling C and t as

$$C = \frac{d}{kY} c, \quad t \sim \frac{1}{\sqrt{kYS}}; \tag{1.4}$$

then the model reduces to

$$\begin{aligned} c &= 1 + \varepsilon\dot{\theta}, \\ \ddot{\theta} + e^{\theta} - 1 &= -\varepsilon\dot{\theta}e^{\theta}, \end{aligned} \tag{1.5}$$

where

$$\varepsilon = \frac{\sqrt{kYS}}{d}. \tag{1.6}$$

This is the equation of a damped nonlinear oscillator, and in starvation conditions such that S is sufficiently small that $\varepsilon \ll 1$, the solutions take the form of slowly

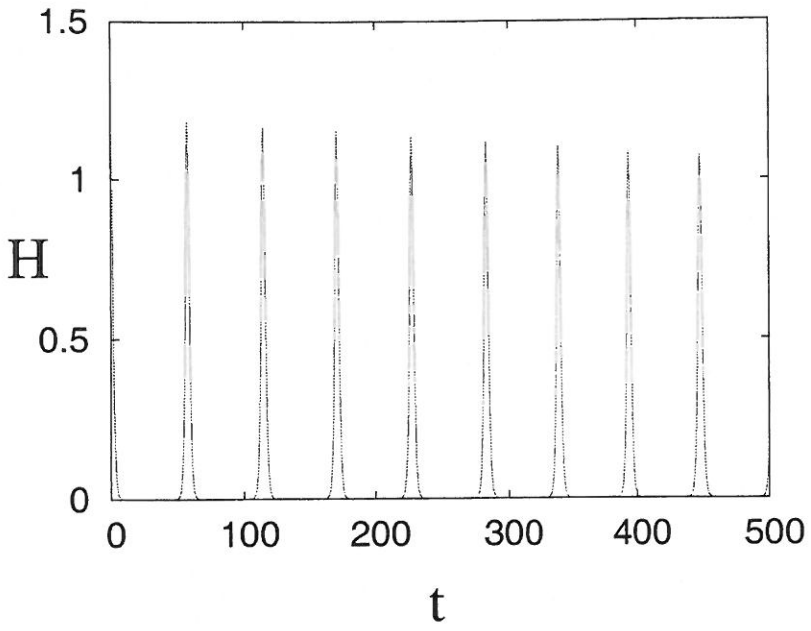

FIG. 1—Solution of (1.2) using ocean calcifier parameter values akin to those of Omta *et al.* ([21]): $S = 0.8 \times 10^{-3}$ mM ka^{-1}, $k = 50$ mM^{-1}, $d = 10^2$ ka^{-1}, $Y = 1$. Here 1 mM $= 10^{-3}$ M, 1 M $= 1$ mole kg^{-1}, and 1 ka $= 10^3$ years. The initial conditions were $C = 2$ mM and $H = 1.2 \times 10^{-4}$ mM. The units of the axes are ka (t) and 10^{-4} mM (H).

decaying oscillations. Figure 1 shows an example obtained from the numerical solution of (1.2). For the parameter values used in this figure, $\varepsilon = 2 \times 10^{-3}$, and the oscillations can be seen to be slowly decaying.

The reason for the spike-like oscillations (and the associated sawtooth oscillations for C) is that the initial conditions are associated with a large value of the dimensionless energy of the undamped nonlinear oscillator in (1.5):

$$E = \tfrac{1}{2}\dot{\theta}^2 + e^{\theta} - \theta, \tag{1.7}$$

and the resulting asymptotic description for $E \gg 1$ is given by Fowler ([4]). This earlier investigation will guide our study below.

Although the model oscillates, ultimately the solutions decay. In seeking to explain observed oscillatory profiles of organic carbon in contaminated soils, Fowler *et al.* ([7]) were led to consider a model of two competing microbial populations, which acts as a generalisation of (1.2), and which acts in a manner similar to an activator–inhibitor system. This model does produce self-sustained, undamped oscillations, and in essence consists of two coupled oscillators similar to (1.5), and indeed the solutions have the same spike-like character. Several questions then arise: what plays the role of the large E in this coupled model, and can we explain as a consequence both why self-sustained oscillations occur, and why they take spike-like form. It is to the solution of these questions that the present paper is devoted.

The rest of the paper is set out as follows. In section 2 we review the competition model for competing microbial populations, and show how it can be recast in the

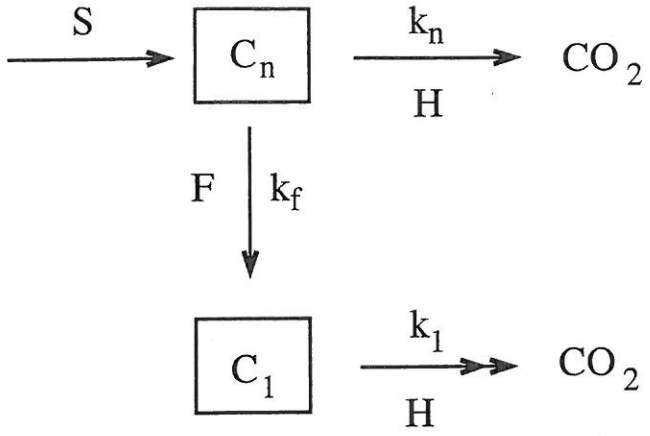

FIG. 2—The schematic competitive reaction scheme between heterotrophs (H) and fermenters (F) which we model.

form of two coupled, weakly damped nonlinear oscillators, using a scaling motivated by that used for (1.2). Numerical solutions show a pronounced spike and sawtooth behaviour. In section 3, we provide a stability analysis which reveals the cause of the self-sustained oscillations. We then give an asymptotic derivation of a three-dimensional Poincaré map which charts the trajectories through two fast phases and two slow phases back to the Poincaré section. Numerical solution of this map indicates that solutions approach a fixed point, corresponding to a periodic solution, and the period and amplitudes of the amplitude spikes are compared to the analytic predictions. The significance of the results is discussed in the concluding section 4.

2. A model of competing microbial populations

The breakdown of organic carbon in the formation of soil, or in the bioremediation of contaminant plumes ([1]), takes place in a number of stages. Complex organic molecules are broken down to sugars by hydrolysis, and these are further broken down by fermentation to produce simpler carbon sources such as acetates ([26]). This stepped process is indicated in Fig. 2, where the supply by hydrolysis is indicated by the supply term S, complex carbons such as sugars are represented as C_n, while simpler carbons are represented by C_1. Different classes of bacteria enable these reactions, with heterotrophs (H) using both forms with respective rate constants k_n and k_1, but preferring the simpler form, so that $k_1 > k_n$. The breakdown of the sugars is enabled by fermentative bacteria F, with rate constant k_f. Mathematical models to describe microbial competition have been investigated by a number of authors over the last forty years (see Smith and Waltman ([25]) for a discussion of the early work), but this has largely focused on competition for a single resource (indicated by taking $k_1 = 0$ in Fig. 2), for which the principle of competitive exclusion applies. (More generally, as we note below when discussing instability, the fermenter population dies out if $k_n > k_f$.) Contradistinctively, we are specifically concerned with the situation where $k_1 > k_n$.

The model scheme in Fig. 2 generalises that of (1.1), to which it reduces if fermentation does not occur ($k_f = 0$). It also effectively becomes a (two-step) linear

process if $k_n = 0$. It has aspects of an activator–inhibitor system, in the sense that use of C_n by H inhibits growth of F, but supply of C_1 by F promotes growth of H. Oscillations can consequently occur, and as we shall see, they become increasingly extreme as the nutrient supply level is reduced: starvation induces boom-and-bust dynamics.

A model to describe the kinetics in Fig. 2 is given by

$$\begin{aligned} \dot{H} &= k_n H C_n + k_1 H C_1 - d_H H, \\ \dot{F} &= k_f C_n F - d_F F, \\ \dot{C}_n &= -\frac{k_f C_n F}{Y_F} - \frac{k_n C_n H}{Y_n} + S, \\ \dot{C}_1 &= \frac{k_f C_n F}{Y_1} - \frac{k_1 H C_1}{Y_H}. \end{aligned} \tag{2.1}$$

If the yield coefficients are all taken to be one, then this corresponds to 'quadratic autocatalysis' as described by Gray and Scott ([9]). Apart from the rate constants k_j, the terms d_k are death rates, and the quantities Y_k are yield coefficients. This model is similar to that of Fowler *et al.* ([7]), except that they assumed Monod reaction terms. Our simpler quadratic reactions reflect conditions of poor nutrient supply, and the difference is largely a cosmetic one.

The equations are scaled similarly as in Fowler *et al.* ([7]), thus

$$H = \frac{S}{d_H} h, \quad F = \frac{S}{d_F} f, \quad C_1 = \frac{d_H}{k_1} c, \quad C_n = \frac{d_F}{k_f} s, \quad t \sim t_0 = \frac{1}{\sqrt{k_f S}}, \tag{2.2}$$

which leads to

$$\begin{aligned} \varepsilon\lambda \dot{h} &= \delta h s + h c - h, \\ \varepsilon \dot{f} &= s f - f, \\ \dot{s} &= \varepsilon \left[1 - \frac{s f}{Y_F} - \frac{\delta h s}{Y_n} \right], \\ \dot{c} &= \varepsilon \delta \kappa \left[\frac{Y_H s f}{Y_1 Y_n} - \frac{h c}{Y_n} \right], \end{aligned} \tag{2.3}$$

where the parameters are defined by

$$\delta = \frac{k_n d_F}{k_f d_H}, \quad \varepsilon = \frac{\sqrt{k_f S}}{d_F}, \quad \lambda = \frac{d_F}{d_H}, \quad \kappa = \frac{k_1 Y_n}{k_n Y_H}. \tag{2.4}$$

Fowler *et al.* ([7]) estimated values of the dimensionless parameters, based on parameter estimates by Langergraber *et al.* ([14]), and found them to be generally of $O(1)$. The exception is the nutrient supply parameter ε, which in conditions of limited nutrient is small; Fowler *et al.* ([7]) estimated $\varepsilon \sim 0.07$. In this case, damped spiking oscillations can occur, indicating an excitable system. However, for certain

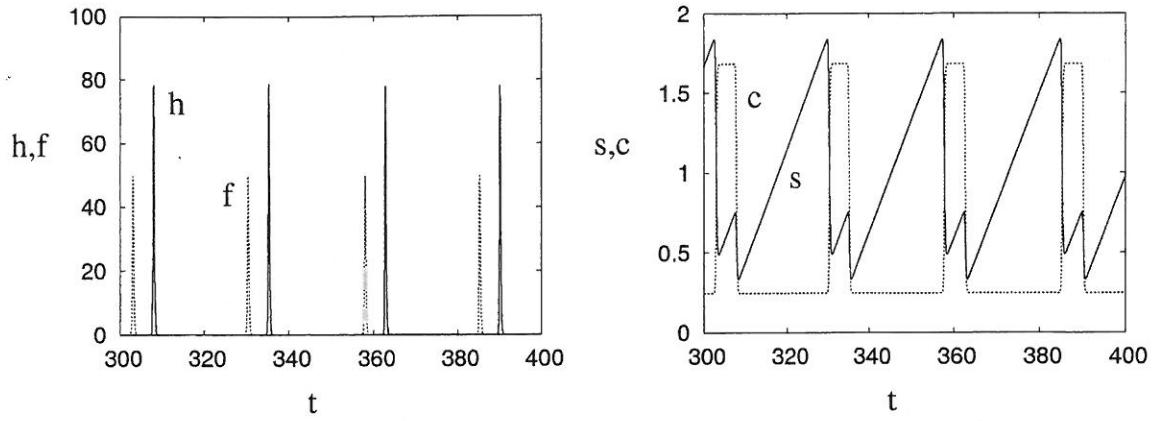

FIG. 3—Numerical solutions of (2.3) with all parameter values set to one except $\delta = 0.5$, $\kappa = 2$ and $\varepsilon = 0.07$. These results use a Runge-Kutta fourth order method with fixed time step 0.001.

parameter values, self-sustained oscillations can occur, and it is these which engage our interest. Our estimate of ε is based on an inferred value of the supply rate S which may be appropriate in contaminated soils, but not in wastewater sites where S would be much larger.

2.1. Numerical solutions

Figure 3 shows numerical solutions of (2.3) with a pronounced asymptotic character. The populations h and f are very spiky, and the minima in Fig. 3 are 2.4×10^{-32} for f and 5.4×10^{-31} for h. As we shall see, this extreme behaviour is associated with the small value of ε. This is reminiscent of similar earlier studies (e. g. Fowler [3]), and is due to the fact that the orbits become almost homoclinic, so that the minima of h and f are exponentially small. It is also reminiscent of an earlier controversy concerning the occurrence of re-emergent (fox) rabies outbreaks, which Murray *et al.* ([20]) represented in a continuous model. Their results were criticised by Mollison ([17]) on the basis that the continuous fox population dwindled to minute fractions of an individual per normal territorial area. The implication of the continuous model should actually be that the population becomes extinct; the same would be true in the present case.

3. Asymptotic solution of the model

We begin our analysis of the model by following the procedure for the simple model (1.2) and defining two 'angle' variables θ and ϕ by

$$f = Y_F e^{\theta}, \quad h = \frac{Y_F Y_H}{Y_1} e^{\phi}. \tag{3.1}$$

It then follows that

$$s = 1 + \varepsilon\dot{\theta}, \quad c = 1 - \delta s + \varepsilon\lambda\dot{\phi}, \tag{3.2}$$

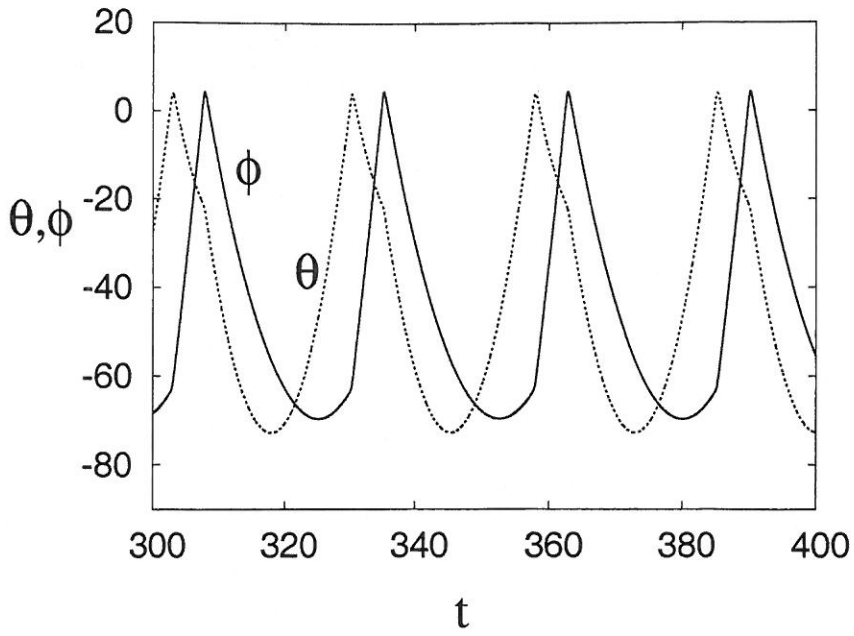

FIG. 4—The solutions for $\theta = \ln f$ and $\phi = \ln h$ (with all $Y_k = 1$), using the same parameters as in Fig. 3. The discontinuities in the gradients occur where h and f spike in Fig. 3, and where c and s jump.

and θ and ϕ satisfy the two coupled oscillator equations

$$\begin{aligned} \ddot{\theta} + e^{\theta} - 1 + \delta^* e^{\phi} &= -\varepsilon\dot{\theta}[e^{\theta} + \delta^* e^{\phi}], \\ \lambda\ddot{\phi} - \delta\ddot{\theta} + \delta^*\kappa[(1-\delta)e^{\phi} - e^{\theta}] &= \varepsilon\delta^*\kappa[\dot{\theta}(e^{\theta} + \delta e^{\phi}) - \lambda\dot{\phi}e^{\phi}], \end{aligned} \tag{3.3}$$

where

$$\delta^* = \frac{\delta Y_F Y_H}{Y_1 Y_n}. \tag{3.4}$$

A first port of call concerns the limits $\delta \to 0$ or $\delta \to \infty$, corresponding to the uncoupling limits $k_n \to 0$ or $k_f \to 0$. The results are similar, although the scaled system (3.3) is more easily analysed for the limit $\delta \to 0$. In this case, the equation $(3.3)_1$ reduces to the weakly damped oscillator $(1.5)_2$, and ϕ is then also a weakly damped oscillator forced by θ. The solutions are oscillatory and spike-like for high E, but ultimately θ and ϕ decay to zero. So the two questions we have to ask are: how does the coupling parameter $\delta > 0$ cause stable oscillations to occur, and how does the only available small parameter ε enable the spike solutions to occur.

3.1. Instability for $\delta > 0$

The answer to the stability question is slightly surprising.

For simplicity we take the yield coefficients to be equal to one, so that $\delta^* = \delta$ in (3.3), and define

$$\mu = \delta^*\kappa. \tag{3.5}$$

The steady state of (3.3) is

$$e^{\phi} = 1, \quad e^{\theta} = 1 - \delta \tag{3.6}$$

(note that this requires $\delta < 1$, and we surmise that for $\delta > 1$, $\theta \to -\infty$, corresponding to $f \to 0$, and the principle of competitive exclusion holds). Linearising about this and seeking modes $\propto e^{\sigma t}$, we obtain the quartic

$$(\sigma^2 + \varepsilon\sigma + 1)\left[\lambda\sigma^2 + \varepsilon\mu\lambda\sigma + \mu(1-\delta)\right] + \delta\left[(\delta - \lambda)\sigma^2 + \varepsilon\mu(1-\lambda)\sigma\right] = 0, \tag{3.7}$$

and clearly both sets of complex conjugate roots have $\operatorname{Re}\sigma = O(\varepsilon) < 0$ when $\delta = 0$.

However, the terms in ε turn out to be largely irrelevant. If we put $\varepsilon = 0$, then (3.7) is simply

$$(\sigma^2 + 1)\left[\lambda\sigma^2 + \mu(1-\delta)\right] + \delta(\delta - \lambda)\sigma^2 = 0, \tag{3.8}$$

and since both roots $\sigma^2 < 0$ for $\delta = 0$, we would expect this to remain true for small positive δ. And indeed this is true; in general the discriminant Δ of (3.8) will remain positive for sufficiently small positive δ.

In more detail, the discriminant of (3.8) is

$$\Delta = [(\lambda + \mu)(1 - \delta) + \delta^2]^2 - 4\mu\lambda(1 - \delta), \tag{3.9}$$

and since we take $\delta < 1$, the roots σ^2 remain negative unless $\Delta < 0$, when they become complex, and instability ensues. For small δ, the condition that $\Delta < 0$ takes the approximate form

$$\delta > \frac{(\lambda - \mu)^2}{2(\lambda^2 + \mu^2)}, \tag{3.10}$$

and is valid for $\lambda \approx \mu$; in particular for $\lambda = \mu$, as in our numerical simulations, this is simply $\delta > 0$; the presence of non-zero ε simply shifts the instability threshold slightly.

3.2. Derivation of a Poincaré map

To answer the question of why the small value of ε causes the solutions to be spiky, we follow the asymptotic procedure which is appropriate for $(1.5)_2$:

$$\ddot{\theta} + e^{\theta} - 1 = 0, \tag{3.11}$$

at large E, as expounded by Fowler ([4]). In essence, the spike solutions are characterised by fast phases, when the exponential dominates, and slow phases, when the exponential is negligible and the algebraic term dominates. Similar behaviour is exhibited for (3.3), whose solutions (corresponding to Fig. 3) are shown in Fig. 4. In a period of the oscillation, there are two fast phases (the f and h spikes) and two slow phases where both exponentials are negligible. We build our analysis around the behaviour shown in Figs 3 and 4.

Standard procedure in asymptotic treatments of relaxation oscillators (e. g. Kevorkian and Cole ([12]), Fowler and Mackey ([5])) is to treat a single slow phase and a single fast phase and match these; the prescription of periodicity is easily

made. In the present case this is not so. The four dimensional system requires determination and matching of three independent variables on a Poincaré section, some of which involves the solution of implicit equations. At best the requirement of periodicity involves a complex set of algebraic equations which must be solved numerically. That being the case, it is more natural, and indeed more general, to construct the relevant Poincaré map on the section and then numerically construct the iterates of the map forward in time. In that way, we not only demonstrate periodicity but show also stability.

To begin the process, we rescale the equations (3.3) by writing

$$\theta = 2\ln\frac{1}{\varepsilon} + \theta^*, \quad \phi = 2\ln\frac{1}{\varepsilon} + \phi^*, \quad t \sim \varepsilon, \tag{3.12}$$

whence the equations are transformed to

$$\begin{aligned} \ddot{\theta} + e^{\theta} + \delta^* e^{\phi} - \varepsilon^2 &= -\dot{\theta}[e^{\theta} + \delta^* e^{\phi}], \\ \lambda\ddot{\phi} - \delta\ddot{\theta} + \delta^*\kappa[(1-\delta)e^{\phi} - e^{\theta}] &= \delta^*\kappa[\dot{\theta}(e^{\theta} + \delta e^{\phi}) - \lambda\dot{\phi}e^{\phi}], \end{aligned} \tag{3.13}$$

where we have dropped the asterisks for convenience. In addition,

$$h = \frac{Y_F Y_H}{\varepsilon^2 Y_1} e^{\phi}, \quad f = \frac{Y_F}{\varepsilon^2} e^{\theta}, \quad s = 1 + \dot{\theta}, \quad c = 1 + \lambda\dot{\phi} - \delta s. \tag{3.14}$$

Key to our analysis is the observation (from Fig. 4, for example) that the peaks of θ and ϕ are separate. There are then three different approximations to be made. The first we take to be where θ is maximum, and we suppose $t = 0$ there; we call this the fast θ phase. There is an equivalent fast ϕ phase, and separating these are slow phases.

Fast θ phase In the fast θ phase, we have $\theta \sim 1$, $-\phi \gg 1$, $t \sim 1$, whence approximately (3.3) gives

$$\begin{aligned} \ddot{\theta} + e^{\theta} &= -\dot{\theta}e^{\theta}, \\ \lambda\ddot{\phi} &= \delta\ddot{\theta} + \delta^*\kappa(1+\dot{\theta})e^{\theta} = (\delta - \delta^*\kappa)\ddot{\theta}. \end{aligned} \tag{3.15}$$

From these there follow

$$[\dot{\phi}]_-^+ = \frac{(\delta - \delta^*\kappa)}{\lambda}[\dot{\theta}]_-^+, \tag{3.16}$$

where $[x]_-^+$ represents the jump in x from $t \to -\infty$ to $t \to +\infty$. In addition, we have the first integral

$$\dot{\theta} - \ln(1+\dot{\theta}) + e^{\theta} = e^{\theta_0}, \tag{3.17}$$

where θ_0 is the maximum. θ is a concave, humped function tending to $-\infty$ at $t = \pm\infty$, and the jump in slope through the fast phase is given by

$$[\dot{\theta} - \ln(1+\dot{\theta})]_-^+ = 0. \tag{3.18}$$

In terms of s and c, we have (using (3.14))

$$[s - \ln s]^+_- = 0, \quad [c]^+_- = -\delta^* \kappa [s]^+_-. \tag{3.19}$$

The calculation of these jumps is sufficient for matching the solution to the slow phases.

Slow phases In the slow phases, both $-\theta$ and $-\phi$ are large, and all the exponentials are negligible. The appropriate rescaling preserving the gradients of θ and ϕ is

$$t = \frac{\tau}{\varepsilon^2}, \quad \theta = \frac{\Theta}{\varepsilon^2}, \tag{3.20}$$

whence (denoting τ derivatives with primes)

$$\Theta'' = 1, \quad \Phi'' = \frac{\delta}{\lambda}, \tag{3.21}$$

and correspondingly

$$s' = 1, \quad c' = 0, \tag{3.22}$$

as is clear in Fig. 3.

Fast ϕ phase This is a little harder, but still possible to do. In the fast ϕ phase, $\phi \sim 1$, $-\theta \gg 1$, $t \sim 1$. The equations (3.3) become approximately

$$\begin{aligned} \ddot{\theta} + \delta^* e^{\phi}(1 + \dot{\theta}) &= 0, \\ \lambda \ddot{\phi} - \delta \ddot{\theta} + \delta^* \kappa [(1 - \delta) + (\lambda \dot{\phi} - \delta \dot{\theta})] e^{\phi} &= 0, \end{aligned} \tag{3.23}$$

from which we can form the first integral

$$\lambda \dot{\phi} - \delta(1 - \kappa)(1 + \dot{\theta}) - \kappa \ln(1 + \dot{\theta}) + \delta^* \kappa \lambda e^{\phi} = L, \tag{3.24}$$

where L is constant, specifically

$$L = \lambda \dot{\phi}_- - \delta(1 - \kappa)(1 + \dot{\theta}_-) - \kappa \ln(1 + \dot{\theta}_-). \tag{3.25}$$

This gives us one jump condition,

$$[\lambda \dot{\phi} - \delta(1 - \kappa)\dot{\theta} - \kappa \ln(1 + \dot{\theta})]^+_- = 0. \tag{3.26}$$

To find another, we write

$$w = \dot{\theta}, \quad \psi = e^{\phi}, \tag{3.27}$$

and then from $(3.23)_1$ and (3.24) we can obtain

$$\lambda \frac{d\psi}{dw} = \frac{\delta^* \kappa \lambda \psi - \{L + \delta(1 - \kappa)(1 + w) + \kappa \ln(1 + w)\}}{\delta^*(1 + w)}, \tag{3.28}$$

with solution

$$\delta^*\lambda\psi = -A(1+w)^\kappa + B - \delta(1+w) + \ln(1+w), \tag{3.29}$$

where A is constant, specifically

$$A = \frac{B - \delta(1+w_-) + \ln(1+w_-)}{(1+w_-)^\kappa}, \tag{3.30}$$

and

$$B = \frac{L+1}{\kappa}. \tag{3.31}$$

Since $s = 1+w$ and $\dot{w} = -\delta^*(1+w)\psi$, it follows that

$$-\lambda\dot{s} = s[-As^\kappa + B - \delta s + \ln s]. \tag{3.32}$$

We need s to tend to a constant at $t = \pm\infty$, so that the right hand side of (3.32) vanishes at $s_\pm$, and this occurs if $A > 0$, and then $[s]_-^+ < 0$, as seen in Fig. 3.

Using (3.24) and (3.31), we can eliminate B to obtain (3.32) in the form

$$-\lambda\dot{s} = s^{1+\kappa}\left[A + \frac{\lambda\dot{\phi} + 1 - \delta s}{\kappa s^\kappa} + \delta\lambda e^\phi\right], \tag{3.33}$$

from which it follows that the second jump condition is

$$\left[\frac{\lambda\dot{\phi} + 1 - \delta s}{s^\kappa}\right]_-^+ = 0. \tag{3.34}$$

Rewriting (3.26) and (3.34) in terms of c and s, we have

$$[c]_-^+ = -\kappa[\delta s - \ln s]_-^+, \quad \left[\frac{c}{s^\kappa}\right]_-^+ = 0. \tag{3.35}$$

3.3. The Poincaré map

We now piece together the solutions through the slow phases with the jumps through the fast phases to obtain a Poincaré map for the flow. We begin just past the maximum of θ, which we take to be at $\tau = 0+$, and we prescribe

$$\Theta' = g_0, \quad \Phi = P_0, \quad \Phi' = p_0 \tag{3.36}$$

at $\tau = 0+$, where $g_0 < 0$, $P_0 < 0$ and $p_0 > 0$. Solving (3.21), we find that

$$\Phi = P_0 + p_0\tau + \frac{\delta}{2\lambda}\tau^2, \quad \Theta = g_0\tau + \tfrac{1}{2}\tau^2, \tag{3.37}$$

whence the value of τ where Φ reaches zero is

$$\tau_P = \frac{\lambda}{\delta}\left[-p_0 + \left(p_0^2 - \frac{2\delta P_0}{\lambda}\right)^{1/2}\right], \tag{3.38}$$

and we have the incoming values

$$\Phi' = p_1 = p_0 + \frac{\delta\tau_P}{2\lambda}, \quad \Theta' = g_1 = g_0 + \tau_P, \quad \Theta = G_1 = g_0\tau_P + \tfrac{1}{2}\tau_P^2. \tag{3.39}$$

The jump across the fast ϕ phase is best done by using (3.35). Specifically, define (see (3.14))

$$s_1 = 1 + g_1, \quad c_1 = 1 + \lambda p_1 - \delta s_1; \tag{3.40}$$

next,

$$K_1 = \frac{c_1}{s_1^\kappa}. \tag{3.41}$$

We then determine s_2 by solving the implicit equation

$$[K_1 s^\kappa + \kappa(\delta s - \ln s)]_1^2 = 0, \tag{3.42}$$

and then we have on the positive side of the jump,

$$c_2 = K_1 s_2^\kappa, \quad \Theta' = g_2 = s_2 - 1, \quad \Phi' = p_2 = \frac{c_2 - 1 + \delta s_2}{\lambda}, \tag{3.43}$$

giving the starting values for the next slow phase (also $\Theta = G_1$).

In the next slow phase, we then have

$$\begin{aligned} \Theta &= G_1 + g_2(\tau - \tau_P) + \tfrac{1}{2}(\tau - \tau_P)^2, \\ \Phi &= p_2(\tau - \tau_P) + \frac{\delta}{2\lambda}(\tau - \tau_P)^2, \end{aligned} \tag{3.44}$$

which determines the location of the next fast θ phase where $\Theta = 0$ at

$$\tau_T = \tau_P - g_2 + \{g_2^2 - 2G_1\}^{1/2}, \tag{3.45}$$

at which point

$$\Phi = P_4 = p_2(\tau_T - \tau_P) + \frac{\delta}{2\lambda}(\tau_T - \tau_P)^2, \tag{3.46}$$

and the incoming values of Θ' and Φ' are

$$\begin{aligned} \Theta' &= g_3 = g_2 + \tau_T - \tau_P, \\ \Phi' &= p_3 = p_2 + \frac{\delta}{\lambda}(\tau_T - \tau_P). \end{aligned} \tag{3.47}$$

Finally, we use (3.18) and (3.16) to compute the values of $\Theta' = g_4$ and $\Phi' = p_4$ on the far side of the θ maximum by solving

$$[g - \ln(1 + g)]_3^4 = 0, \tag{3.48}$$

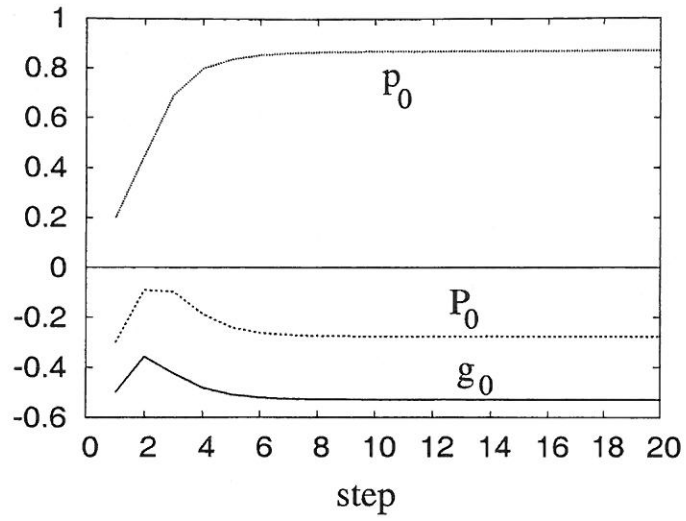

FIG. 5—Iteration of the approximate Poincaré map applied to the parameters g_0, p_0 and P_0. The iterates converge to the steady values $g_0 = -0.53$, $p_0 = 0.87$, $P_0 = -0.28$.

and then

$$[p]_3^4 = \frac{(\delta - \delta^*\kappa)}{\lambda}[g]_3^4. \tag{3.49}$$

This completes the derivation of the Poincaré map, which maps coordinates $g_0 < 0$, $P_0 < 0$, $p_0 > 0$ on the (approximate) Poincaré surface $\Theta \approx 0$ to subsequent values g_4, P_4, p_4. The solution must be obtained numerically, because both (3.42) and the similar (3.48) must be solved numerically. If the solutions tend towards a fixed point, then this corresponds to a periodic solution with period (in τ) equal to τ_T.

3.4. Numerical computation of the Poincaré map

Numerical investigation of the iterates of the Poincaré map is straightforward, with the only issue being the necessity (twice) to solve the equation

$$F(s, K, \mu, \delta) = F(s_0, K, \mu, \delta), \tag{3.50}$$

where

$$F = Ks^\mu + \mu(\delta s - \ln s), \tag{3.51}$$

and the unique root $s < s_0$ is sought. This is done using Newton's method, and by taking an initial guess for s such that $F(s) > F(s_0)$ and $0 < s < s_0$.

Numerical calculation of the Poincaré map indicates that, as we expect, the iterates rapidly approach a fixed point (see Fig. 5). We assess the accuracy of the asymptotic method by charting the period P (in τ) and the maxima and minima of the four variables h, f, s and c. In terms of the quantities described above, these are given, after convergence to the fixed point of the map, by

$$P = \tau_T, \quad c_{\max} = c_1, \quad c_{\min} = c_2, \quad s_{\max} = s_3, \quad s_{\min} = s_2. \tag{3.52}$$

The minima of h and f are given from (3.14) and (3.20) by

$$h_{\min} = \frac{Y_F Y_H}{\varepsilon^2 Y_1} \exp\left(\frac{\Phi_{\min}}{\varepsilon^2}\right), \quad f_{\min} = \frac{Y_F}{\varepsilon^2} \exp\left(\frac{\Theta_{\min}}{\varepsilon^2}\right), \tag{3.53}$$

and from (3.44) we have

$$\Theta_{\min} = G_1 - \tfrac{1}{2} g_2^2, \quad \Phi_{\min} = -\frac{\lambda p_2^2}{2\delta}. \tag{3.54}$$

The maximum of f is given from (3.14) and (3.17) by

$$f_{\max} = \frac{Y_F}{\varepsilon^2}[g_3 - \ln(1 + g_3)], \tag{3.55}$$

but the maximum of ϕ requires a little more effort. The values of s and $\psi = e^{\phi}$ at the maximum are given by (3.24) and (3.29), where the constants L, B and A are given by (3.25), (3.31) and (3.30), which can be written in the form

$$L = \lambda p_1 - \delta(1 - \kappa) s_1 - \kappa \ln s_1, \quad B = \frac{L + 1}{\kappa}, \quad A = \frac{B - \delta s_1 + \ln s_1}{s_1^{\kappa}}. \tag{3.56}$$

Eliminating ψ, we find s by solving

$$\kappa A s^{\kappa} + \delta s - 1 = 0, \tag{3.57}$$

and then

$$h_{\max} = \frac{Y_n}{\varepsilon^2}\left[\frac{B - (As^{\kappa} + \delta s - \ln s)}{\delta \lambda}\right], \tag{3.58}$$

using the definition of δ^* in (3.4).

Table 1 shows a comparison of the analytic predictions with the values from direct numerical solution. The asymptotic approach of the numerical solutions is fairly clear. The apparent inaccuracy in the first four rows (particularly the minima) is due to the exponential divergence of the results with ε. The results for ϕ and θ clearly show the consistency of the numerical and asymptotic results.

Obviously the minima in the microbial populations $h_{\min}$ and $f_{\min}$ become extremely small as ε is reduced. To relate these values to actual microbial densities, we need to calculate the corresponding quantities

$$H_{\min} = \frac{S h_{\min}}{d_H}, \quad F_{\min} = \frac{S f_{\min}}{d_F}. \tag{3.59}$$

Fowler *et al.* ([7, table 1]) assumed values

$$S \sim 0.4 \times 10^{-4} \text{ mg COD l}^{-1} \text{ d}^{-1}, \quad d_H \sim 0.2 \text{ d}^{-1}, \quad d_F \sim 0.02 \text{ d}^{-1}, \tag{3.60}$$

from which we have

$$\frac{S}{d_H} \sim 2 \times 10^{-4} \text{ mg}_{\text{COD}} \text{ l}^{-1}, \quad \frac{S}{d_F} \sim 2 \times 10^{-3} \text{ mg COD l}^{-1}. \tag{3.61}$$

ε	0.2		0.07		0.05	
	num	as	num	as	num	as
$h_{\max}$	12.1	7.81	0.78×10^{2}	0.64×10^{2}	0.15×10^{3}	0.13×10^{3}
$h_{\min}$	0.19×10^{-3}	0.98×10^{-2}	0.54×10^{-30}	0.32×10^{-25}	0.18×10^{-59}	0.12×10^{-51}
$f_{\max}$	7.40	5.6	0.50×10^{2}	0.46×10^{2}	0.96×10^{2}	0.90×10^{2}
$f_{\min}$	0.75×10^{-4}	0.49×10^{-2}	0.24×10^{-31}	0.11×10^{-27}	0.99×10^{-62}	0.19×10^{-56}
P	2.242		1.922		1.897	1.797
$\phi_{\max}$	−0.73		−0.96		−0.98	−1.163
$\Phi_{\min}$	−0.47		−0.37		−0.36	−0.314
$\theta_{\max}$	−1.22		−1.41		−1.43	−1.496
$\Theta_{\min}$	−0.51		−0.38		−0.37	−0.342
$s_{\max}$	1.796		1.835		1.840	1.826
$s_{\min}$	0.361		0.332		0.325	0.323
$c_{\max}$	1.862		1.683		1.662	1.560
$c_{\min}$	0.211		0.246		0.249	0.278

TABLE 1—Values of various asymptotically determined quantities compared with the numerical solutions at differing values of ε, and the analytic prediction. Values of the other parameters are all one except $\delta = 0.5$ and $\kappa = 2$. For clarity, where the asymptotic values are independent of ε (at leading order), the asymptotic result is only shown in the right hand column.

The units of bacterial biomass are taken as mg l^{-1} of chemical oxygen demand (COD) (Metcalf and Eddy ([16])), which is measured from an assay in which oxygen consumption is determined. Bacterial biomass is not often measured *per se*. In order to relate COD to actual cell numbers, we use the measurements of Münch and Pollard ([18]), who estimate a value for wastewater and wastewater sludges of 0.2×10^{-9} mg $_{\text{COD}}$ cell^{-1}. In soils, bacterial cell density is commonly $\sim 10^{11}$–10^{12} cells l^{-1} (Raynaud and Nunan ([22])), suggesting biomass density ~ 10–10^{2} mg $_{\text{COD}}$ l^{-1}, while extreme or inhospitable environments have a factor of 10^{6} less (Kirchman ([13, p. 9])), corresponding to $\sim 10^{-5}$–10^{-4} mg $_{\text{COD}}$ l^{-1}. At face value, this suggests paradoxically that the extinction we envisage does not practically occur.

The issue is occluded, however, because bacterial populations are not like, say, fox populations, insofar as they do not really completely die out. In conditions of low nutrient supply, bacterial cells may enter a dormant state in which they can survive for very long times, and for that reason the continuous model where repeated outbreaks occur does make sense insofar as there is an extra dormant state analogous to the removed population in an S–I–R model (e. g. Murray [19]). A fraction of the microbes will survive in this dormant state until nutrient conditions improve for the next bloom period. The fact that the active microbe population dwindles to near zero is not then of concern, except that it will be the size of the dormant population which controls the size of the next outbreak.

4. Conclusions

In this paper we have studied a simple but realistic model for oscillations in microbial populations, which has surprising characteristics. A single population supplied by limited nutrient will undergo transient boom-and-bust kinetics before finally relaxing to equilibrium. However, when two interacting populations with a degree of syntrophy are placed in similar starvation conditions, their interaction can promote self-sustained oscillations, and these oscillations can exhibit extraordinarily low values of the populations, sufficient to warrant the actual extinction of the populations. It is of some mathematical interest to understand the cause of these extinctive minima, and we have shown that the minima are exponentially small in terms of the small starvation parameter. In practice, the appearance of oscillations is the harbinger of doom for the populations. A similar feature occurs in some other situations; for example the occurrence of waves in two-phase bubbly flows may herald the breakdown of the flow régime, and the formation of slug flow ([23]).

In practice, if such oscillations were to occur, we would not expect such extreme variation, and this would also imply less severe oscillations in the chemical nutrients.

A novel feature of the oscillations is the fact that the two populations have their peak at different times in the oscillation. The apparent reason is that it is the rise of the fermenter population which enables the (later) rise of the heterotrophs, much as in the antigen-antibody interaction in the immune system ([2]). Assuming this is a generic feature, it raises the possibiity that more complex models involving sequences of interacting populations will exhibit oscillations involving multiple spikes; however, it also seems reasonable to suggest that the occurrence of oscillating populations in itself acts as a warning that such populations are susceptible to extinction.

Acknowledgements

Thanks to Laura Cribbin, Henry Winstanley, Sarah Mitchell, Stephen O'Brien and Alan Hegarty for advice and discussion. I acknowledge the support of the Mathematics Applications Consortium for Science and Industry (www.macsi.ul.ie) funded by the Science Foundation Ireland mathematics initiative grant 12/1A/1683. This publication has emanated from research conducted with the financial support of Science Foundation Ireland under Grant Number: SFI/09/IN.1/I2645.

References

[1] F.H. Chapelle, *Groundwater microbiology and geochemistry*, Wiley, 2nd edn, 2001.

[2] A.C. Fowler, Approximate solution of a model of biological immune responses incorporating delay, *Journal of Mathematical Biology* **13** (1981), 23–45.

[3] A.C. Fowler, An asymptotic analysis of the logistic delay equation when the delay is large, *IMA Journal of Applied Mathematics* **28** (1982), 41–9.

[4] A.C. Fowler, Note on a paper by Omta *et al.* on sawtooth oscillations, *SeMA Journal* **62** (2013), 1–13.

[5] A.C. Fowler and M.C. Mackey, Relaxation oscillations in a class of delay-differential equations, *SIAM Journal on Applied Mathematics* **63** (1) (2002), 299–323.

[6] A.C. Fowler and M.J. McGuinness, A description of the Lorenz attractor at high Prandtl number, *Physica* **5D** (1982), 149–82.

[7] A.C. Fowler, H.F. Winstanley, M.J. McGuinness and L.B. Cribbin, Oscillations in soil bacterial redox reactions, *Journal of Theoretical Biology* **342** (2014), 33–8.

[8] A. Goldbeter, *Biochemical oscillations and cellular rhythms*, Cambridge University Press, Cambridge, 1996.

[9] P. Gray and S.K. Scott, *Chemical oscillations and instabilities: non-linear chemical kinetics*, Clarendon Press, Oxford, 1994.

[10] J. Keener and J. Sneyd, *Mathematical physiology. I: cellular physiology*, Springer-Verlag, New York, 2009.

[11] W.O. Kermack and A.G. McKendrick, Contributions to the mathematical theory of epidemics, *Proceedings of The Royal Society of London. Series A* **115** (1927), 700–21.

[12] J. Kevorkian and J.D. Cole, *Perturbation methods in applied mathematics*, Springer-Verlag, Berlin, 1981.

[13] D.L. Kirchman, *Processes in microbial ecology*, Oxford University Press, Oxford, 2012.

[14] G. Langergraber, D.P.L. Rousseau, J. Garcia and J. Mena, CWM1: a general model to describe biokinetic processes in subsurface flow constructed wetlands, *Water Science and Technology* **59** (2009), 1687–97.

[15] A. Mahadevan, E. D'Asaro, M.-J. Perry and C. Lee, Eddy-driven stratification initiates North Atlantic Spring phytoplankton blooms, *Science* **337** (6090) (2012), 54–8.

[16] Metcalf & Eddy Inc., *Wastewater engineering: treatment, disposal, and reuse*, 4th international edn, McGraw-Hill, New York, 2004.

[17] D. Mollison, Dependence of epidemic and population velocities on basic parameters, *Mathematical Biosciences* **107** (1991), 255–87.

[18] E.V. Münch and P.C. Pollard Measuring bacterial biomass-COD in wastewater containing particulate matter, *Water Resources* **31** (10) (1997), 2550–6.

[19] J.D. Murray, *Mathematical biology*, Springer-Verlag, Berlin, 1993.

[20] J.D. Murray, E.A. Stanley and D.L. Brown, On the spatial spread of rabies among foxes, *Proceedings of The Royal Society of London. Series B* **229** (1986), 111–50.

[21] A.W. Omta, G.A.K. van Voorn, R.E.M. Rickaby and M.J. Follows, On the potential role of marine calcifiers in glacial-interglacial dynamics, *Global Biogeochemical Cycles*, **27** (2013), 692–704.

[22] X. Raynaud and N. Nunan, Spatial ecology of bacteria at the microscale in soil, *Plos One* **9** (1) (2014), e87217.

[23] M. Robinson, A.C. Fowler, A.J. Alexander and S.B.G. O'Brien, Waves in Guinness, *Physics of Fluids* **20** (2008), 067101.

[24] X. Sanchez-Vila, S. Rubol, A. Carles-Brangari and D. Fernàndez-Garcia, An analytical solution to study substrate-microbial dynamics in soils, *Advances in Water Resources* (54) (April 2013), 181–90. doi: 10.1016/j.advwatres.2013.02.004

[25] H.L. Smith and P. Waltman, *The theory of the chemostat: dynamics of microbial competition*, Cambridge University Press, 1995.

[26] M. Thullner, P. Regnier and P. Van Cappellen, Modeling microbially induced carbon degradation, in redox-stratified subsurface environments: concepts and open questions, *Geomicrobiology Journal* **24** (2007), 139–55.